Research on Accessibility Factors of Metal Particles and Structural Optimization of Intermediate Gearbox in a Helicopter

*LU Fengxia**, *WANG Honglin*, *WEI Kun*, *LENG Sheng*

National Key Laboratory of Science and Technology on Helicopter Transmission, Nanjing University of Aeronautics and Astronautics, Nanjing 210016, P. R. China

(Received 10 April 2024; revised 23 September 2024; accepted 15 October 2024)

Abstract: The intermediate gearbox of a helicopter operates under splash lubrication. If the bearing produces metal particles due to insufficient lubrication or wear, whether it can be adsorbed by the metal particles signal at the bottom of the gearbox and alarm directly affects the flight safety of the helicopter. Based on the CFD method, the factors affecting the accessibility of metal particles are analyzed by using the volume of fluid-discrete phase model (VOF-DPM) coupling model, the RNG k-ε turbulence model and the dynamic grid technology. Furthermore, the optimization research on the casing structure is conducted. Experimental results show that the accessibility of metal particles is optimal when the gear speed is 6 000 rad/min or the immersion depth is 24 mm. The density of metal particles exhibits a nonlinear relationship with their accessibility, and the particle size has a relatively small impact on their accessibility without an order of magnitude change.

Key words: intermediate gearbox; splash lubrication; metal particles; CFD; three-phase flow

CLC number: TH132.46 **Document code**: A **Article ID**: 1005-1120(2024)06-0766-17

0 Introduction

During the operation of the helicopter, the intermediate gearbox operates under splash lubrication, and metal particles appear at the internal bearings and raceways due to wear and tear, which flows into the gearbox with oil and gas. If the metal particles touch the bottom of the oil pool and are adsorbed by the metal particles signal, it will alarm to meet the accessibility fault monitoring requirements. However, if metal particles deposit on the casing wall surface with the flow of oil and gas, causing bearing failures to be detected promptly, it will affect the flight safety and service life of the helicopter.

In hydrodynamics study, theoretical methods can be used to analyze two-phase flow problems, such as microscopic analysis theory based on the Boltzmann equation and the statistical averaging method, or the macroscopic analysis theory based on establishing phase equation. These two methods are difficult to solve and have limitations in engineering applications. With the advancement of computer technology, the CFD method has become a mature technique for solving two-phase flow problems. It not only provides a new approach for theoretical methods to solve complex flow problems, but also has a lower economic cost.

Based on the volume of fluid (VOF) model and turbulence model, Jiang et al.[1] established a subtractive numerical calculation model for splash lubrication by using the CFD method, and studied the lubrication flow field characteristics. Luo et al.[2] used high-speed cameras to capture the movement trajectory of lubricating oil in complex gearboxes with splash lubrication to verify the accuracy of the simulation. Peng et al.[3] proposed the tooth surface

*Corresponding author, E-mail address: meefxlu@nuaa.edu.cn.

How to cite this article: LU Fengxia, WANG Honglin, WEI Kun, et al. Research on accessibility factors of metal particles and structural optimization of intermediate gearbox in a helicopter[J]. Transactions of Nanjing University of Aeronautics and Astronautics, 2024, 41(6): 766-782.

http://dx.doi.org/10.16356/j.1005-1120.2024.06.008

movement method to deal with the mesh division difficulty caused by small meshing position clearance in the numerical modelling process of gear splash lubrication. The comparison between the simulated gear resistance moment and experimental results shows that using the separation method and the tooth surface movement method is more accurate. Liu et al.[4] established a gearbox model and used the CFD method and VOF model to simulate and analyze the internal flow field of the gearbox, calculating the dynamic characteristics of the flow field of the gearbox at different speeds. Dong et al.[5] used the CFD method to analyze the internal flow field of the splash lubrication gearbox, and studied the instantaneous oil distribution, as well as the changes in flow field pressure and flow rate. Zhang[6] used the transient method to simulate the flow field of the intermediate gearbox and analyzed the effects of fluid velocity, pressure distribution, and rotational speed on the internal flow field. Wang[7] simulated and analyzed the bevel gearbox, and discussed the effects of parameters such as lubricating oil viscosity and gear speed. Liu et al.[8] established a CFD model based on the particle method to study the distribution of lubricating oil and the power loss of oil stirring in the gearbox, and conducted experimental verification, showing good consistency. Li et al.[9] studied the gas-liquid two-phase flow inside the gearbox using the CFD method and conducted visualization experiments using high-speed cameras, and the results showed good consistency. Peng et al.[10] proposed a numerical method for simulating and analyzing splash lubrication in a quasi-hyperbolic gearbox based on the CFD method, and obtained consistent lubricating oil flow field and stirring power loss in the gearbox through experiments. Xu et al.[11] controlled the splashing oil flow through a shield to achieve directional oil delivery, in order to solve the problem of insufficient lubrication capacity of the splashing lubrication system in the drive axle main reducer (DAMR) caused by long-distance rapid oil supply to the bearings.

At present, the technology of tracking particle phase trajectories using CFD methods has been applied in the fields of chemical engineering and environment, mainly in the background of dust removal, pipeline transportation, separators, centrifugal pumps, fluidized beds, etc. However, there are few related research contents that focus on complex transmission systems.

Hu et al.[12] established a fluid-solid coupling model for a curved pipe using the CFD-discrete phase model (CFD-DPM) coupling method, obtained the trajectory of solid particle motion, and combined it with the particle collision model to analyze the impact of particle motion on the erosion of the curved pipe wall. This allowed for the identification of erosion damage areas and failure forms, discussed the effects of different working conditions, and curved pipe structural parameters and medium flow conditions on erosion failure. He et al.[13] used the Euler multiphase flow model to analyze the flow field inside the solid-liquid two-phase flow slide valve and conducted a 2-D numerical simulation. Qin et al.[14] established a three-phase flow field system with glycerol solution as the liquid phase and sand and red mud as the solid phase. The conductivity method was used to measure the mixing time of the three-phase flow field, and CFD numerical simulation calculations were conducted based on the Euler multiphase flow model. Zhao et al.[15] used the CFD-DPM coupled model numerical method to study the internal flow field of a disc separator and track the motion trajectory of its particles. Sun[16] used the DPM-VOF coupling method to numerically simulate the motion characteristics of PM2.5/PM10 microparticles in the monitoring system. Based on the solid-liquid two-phase flow, the VOF-DPM coupling model was used to study the effects of factors such as inlet velocity, liquid viscosity, liquid density, and gas-liquid surface tension on the trajectory of microparticles in gas-liquid-solid three-phase flow. Peng et al.[17] used the CFD-DPM coupling method to numerically simulate the solid-gas two-phase flow characteristics in a cyclone separator, and studied the effects of operating conditions and structural parameters on the performance of the cyclone separator. Zhang et al.[18] established a CFD model for oil-water particle three-phase flow based on the VOF-DEM model to study the particle transport and accumulation behavior after fracture water

flooding. Gao et al.[19] used CFD and discrete element method (DEM) coupling methods to study a novel quantitative seed feeding system, analyzed the flow behavior of seed particles and airflow field in the system, and investigated the effects of different variables related to the Venturi tube and operation. Wang et al.[20] numerically simulated the motion of discrete phase particles in a screw conveyor based on the DPM model, studied the particle flow behavior and transportation status of the screw conveyor at different screw speeds and volume fractions, and predicted the particle velocity and spatial distribution. The combination of DPM and direct numerical simulation (DNS) proposed by Zhang et al.[21] has been widely used in gas-solid flow simulation. Pan et al.[22] reviewed the current theoretical and experimental work on three-phase fluidized bed reactors (FBRs) and analyzed the application of CFD methods in three-phase fluidized bed systems. Yang et al.[23] studied particle motion in supersonic flow with strong swirling flow using a DPM model. Sun et al.[24] used the CFD method to study erosion at pipeline bends caused by gas-solid two-phase flow, and used the direct simulation Monte Carlo (DSMC) method to study the effects of key factors such as particle collisions and particle concentration distribution on erosion ratio. Song et al.[25] used the CFD method to study the motion of solid particles in a cyclone separator. The results were applied to the stochastic Lagrangian particle tracking (LPT) model to simulate particle motion, and the applicability of the simulation model was verified through comparison with experiments. Ref.[26] proposed a side blown vortex melt reduction reactor and conducted numerical simulation of multiphase flow in the furnace. The influence of nozzle diameter and corrected Froude number on the interaction between coal gas, copper slag, and iron was studied. Ref.[27] studied the effects of detonation conditions on detonation wave propagation and engine performance in pulse detonation engines. They used the adaptability of the adaptive mesh refinement method in detonation-based engines, reducing the average total cell count by a factor of 2.617, and obtaining consistent results according to validation studies.

With the advancement of computer technology, the CFD method has become a mature technique for solving two-phase flow. In the past few decades, the application of CFD in the aviation field has had a profound impact on aircraft design, reducing the dependence on wind tunnels to a certain extent[28]. The existing research on multiphase flow containing particle phases mainly focuses on studying the motion characteristics of particle phases and analyzing the wear of the system. However, there are few related research that focus on particle phases aimed at real-time monitoring of system faults, and the accessibility of particle phases. To reveal the settling mechanism and accessibility law of the metal chips, this paper applies the CFD method to simulate the three-phase flow of air, oil, and metal chips in the intermediate gearbox. It predicts the distribution of oil in the casing, the motion state of the fluid, and the trajectory of the metal chips, avoiding their deposition on the casing wall, and providing technical methods for fault monitoring and structural optimization in the intermediate gearbox.

1 Simulation Calculation Method for Accessibility of Metal Particles in Solid-Liquid-Gas Three-Phase Flow

1.1 Governing equation

The three-phase flow inside the intermediate gearbox is a complex and disordered turbulent motion, but it also follows the basic N-S equation[29].

(1) The mass conservation equation is

$$\frac{\partial(\rho u)}{\partial x}+\frac{\partial(\rho v)}{\partial y}+\frac{\partial(\rho w)}{\partial z}=0 \tag{1}$$

where ρ is the fluid element density, kg/m^3; and t the time, s; u, v, and w are the velocity components of the fluid element, m/s.

(2) The momentum conservation equations are

$$\frac{\partial(\rho u)}{\partial t}+\frac{\partial(\rho uu)}{\partial x}+\frac{\partial(\rho uv)}{\partial y}+\frac{\partial(\rho uw)}{\partial z}=$$
$$-\frac{\partial p}{\partial x}+\frac{\partial \tau_{xx}}{\partial x}+\frac{\partial \tau_{yx}}{\partial y}+\frac{\partial \tau_{zx}}{\partial z}+F_x \tag{2}$$

$$\frac{\partial(\rho v)}{\partial t}+\frac{\partial(\rho vu)}{\partial x}+\frac{\partial(\rho vv)}{\partial y}+\frac{\partial(\rho vw)}{\partial z}=$$
$$-\frac{\partial p}{\partial y}+\frac{\partial \tau_{xy}}{\partial x}+\frac{\partial \tau_{yy}}{\partial y}+\frac{\partial \tau_{zy}}{\partial z}+F_y \quad (3)$$

$$\frac{\partial(\rho w)}{\partial t}+\frac{\partial(\rho wu)}{\partial x}+\frac{\partial(\rho wv)}{\partial y}+\frac{\partial(\rho ww)}{\partial z}=$$
$$-\frac{\partial p}{\partial z}+\frac{\partial \tau_{xz}}{\partial x}+\frac{\partial \tau_{yz}}{\partial y}+\frac{\partial \tau_{zz}}{\partial z}+F_z \quad (4)$$

where $\tau_{xx}=2\mu\frac{\partial u}{\partial x}-\frac{2}{3}\left(\frac{\partial u}{\partial x}+\frac{\partial v}{\partial y}+\frac{\partial w}{\partial z}\right)$

$$\tau_{yy}=2\mu\frac{\partial v}{\partial y}-\frac{2}{3}\left(\frac{\partial u}{\partial x}+\frac{\partial v}{\partial y}+\frac{\partial w}{\partial z}\right)$$

$$\tau_{zz}=2\mu\frac{\partial w}{\partial z}-\frac{2}{3}\left(\frac{\partial u}{\partial x}+\frac{\partial v}{\partial y}+\frac{\partial w}{\partial z}\right)$$

$$\tau_{xy}=\tau_{yx}=\mu\left(\frac{\partial u}{\partial y}+\frac{\partial v}{\partial x}\right)$$

$$\tau_{xz}=\tau_{zx}=\mu\left(\frac{\partial u}{\partial z}+\frac{\partial w}{\partial x}\right)$$

$$\tau_{yz}=\tau_{zy}=\mu\left(\frac{\partial v}{\partial z}+\frac{\partial w}{\partial y}\right)$$

p is the pressure on the fluid element, Pa; and μ the dynamic viscosity, Pa·s. F_x, F_y, and F_z are the physical forces on the fluid element, $kg\cdot m^{-2}s^{-2}$; and τ_{xx}, τ_{yy}, τ_{zz}, τ_{xy}, τ_{yx}, τ_{xz}, τ_{zx}, τ_{yz}, and τ_{zy} the viscous stress components on the surfaces of the fluid elements, Pa.

1.2 Solid-liquid-gas three-phase flow model

The main numerical calculation methods for multiphase flow include the Euler-Euler coupling method and the Euler-Lagrange coupling method. The Euler-Euler coupling method treats all phases as continuous phases and solves them based on the Euler coordinate system. The Euler-Lagrangian coupling method treats the fluid phase as a continuous phase and the particle phase as a discrete phase, which solves the fluid phase in the Euler coordinate system and simulates the flow characteristics of the fluid. And in the Lagrangian coordinate system, the dispersion phase is solved to obtain the motion trajectory of particles.

For cases where the volume fraction of discrete phases is less than 10%—12%[30], the DPM model can be used to treat particles as particles. Based on the Lagrangian coordinate system, the interaction forces, collisions, friction, deformation, etc. between particles are ignored. The Newton's second law is used to calculate the motion trajectory of particles in the flow field, and the motion balance equation of particles is obtained as

$$m_p\frac{du_p}{dt}=m_p\frac{u-u_p}{\tau_r}+m_p\frac{g(\rho_p-\rho)}{\rho_p}+F \quad (5)$$

where m_p is the mass of particles, kg; u the velocity of the continuous phase, m/s; u_p the particle velocity, m/s; $m_p(u-u_p)/\tau_r$ the fluid drag force on the particle, N; ρ_p the density of particles, kg/m^3; ρ the density of the continuous phase, kg/m^3; $m_pg(\rho_p-\rho)/\rho_p$ the combined force of gravity and buoyancy on particles; F the additional force, N; τ_r the relaxation time of the particle, s, shown as[31]

$$\tau_r=\frac{\rho_p d_p^2}{18\mu_0}\frac{24}{C_d Re} \quad (6)$$

where μ_0 is the molecular viscosity of the continuous phase, Pa·s; d_p the particle diameter, m; Re the relative Reynolds number; C_d the resistance coefficient, shown as

$$C_d=a_1+\frac{a_2}{Re}+\frac{a_3}{Re^2} \quad (7)$$

where a_1, a_2 and a_3 are the constants, with different values within different Reynolds number ranges[32].

In addition to being subjected to fluid buoyancy, fluid drag, and particle gravity in the flow field, particles are also subjected to other additional surface forces due to the relative motion between the fluid and particles and the viscosity of the fluid itself, namely F in Eq.(5). According to the type of particle loading, the forces are divided into the following types: Gravity and buoyancy, aerodynamic drag (fluid drag), virtual mass force, pressure gradient force, thermophoretic force, Brownian force, Saffman lift, Magnus lift, etc. When calculating, consider adding three additional forces: Virtual mass force, pressure gradient force, and Magnus lift.

1.3 Intermediate gearbox model

The subtractive structure is shown in Fig.1. When the gearbox is just starting, the lubricating oil is distributed at the bottom of the gearbox. After the

spiral bevel gear rotates at high speed, the lubricating oil is stirred and splashed to the meshing point of the tooth surface to lubricate and cool the gear. However, the bearing is far from the gear and the lubricating oil makes it difficult to fully lubricate the bearing. Therefore, a guide pipe is set on the end cover to drain the lubricating oil to the bearing, and then the lubricating oil is returned to the interior of the gearbox through the oil return port at the bottom of the end cover, to lubricate and cool the bearing. However, the lubrication effect of the bearings is still poor, and they are prone to wear due to insufficient lubrication. Metal particles flow with oil and gas to the inside of the gearbox.

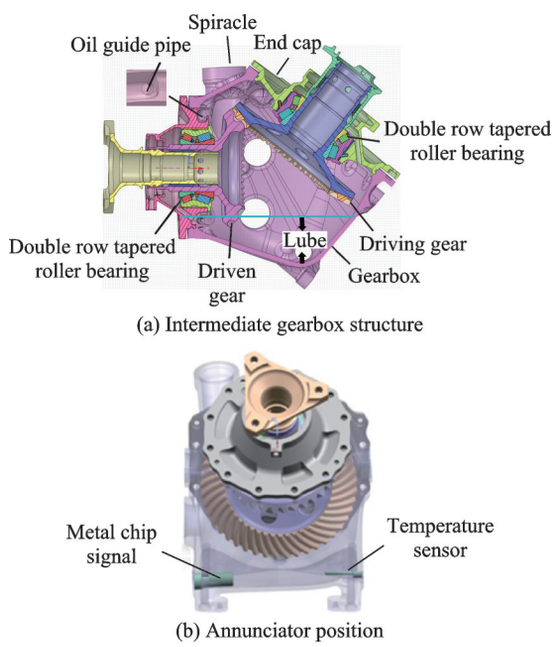

Fig.1 Schematic diagram of intermediate gearbox structure

In the calculation example of this article, the parameters of the spiral bevel gear are shown in Table 1, and the main parameters of the bearing and metal particles are shown in Table 2.

Table 1 Main parameters of spiral bevel gears

Parameter	Driving wheel	Driven wheel
Rotation direction	Right	Left
Number of teeth	31	43
Modulus m/mm	3.8	3.8
Tooth width b/mm	25	25
Pressure angle α/(°)	20	20
Helix angle β/(°)	30	30
Crossed axis angle Σ/(°)	128	128

Table 2 Main parameters of bearings and metal particles

Parameter	Input bearing	Output bearing
Number of rollers	22/25	22/25
Inner circle speed/(r•min^{-1})	5 000	3 804
Small roller speed/(r•min^{-1})	2 264.05	1 722.65
Large roller speed/(r•min^{-1})	2 228.82	1 695.84
Inner ring diameter d/mm	55	55
Outer ring diameter d/mm	90	90
Bearing width b/mm	40	40
Metal particle size/mm	0.72	0.72
Metal scrap material	M50-NiL	M50-NiL
Metal particles density ρ/(kg•m^{-3})	7 810	7 810

1.4 CFD simulation settings

Divide a tetrahedral unstructured mesh into a computational model for the complex structure of the reduced flow field. To prevent negative volume during dynamic mesh calculation, local refinement of the mesh is carried out in the vicinity of the bevel gear to ensure that there are at least two layers of mesh at the gap during the boundary motion of the bevel gear. The ventilation holes and oil return ports also need to undergo local mesh refinement, while the rest are divided into global unstructured grids, as shown in Fig.2.

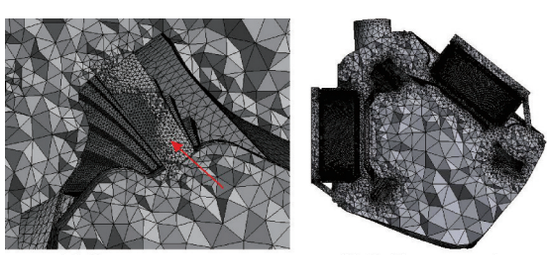

Fig.2 Grid division results

To eliminate the impact of grid size on the calculation results, monitor the flow rate of the ventilation holes and verify grid independence. When the number of grids is about 1.35 million, the flow gradient of the ventilation holes tends to stabilize. Therefore, the number of grids in the reduced model is determined to be 1 384 768, with a minimum mesh size of 0.6 mm and a maximum slope of 0.728 8, which meets the calculation standards.

Considering the calculation cost, this article only sets the falling position of metal particles at the long row conical bearings (Fig.3), and places 10

metal particles at the driving and driven gear bearings, named pinions 1—10 and gears 1—10, respectively. Their initial velocity vectors are shown in Fig.4.

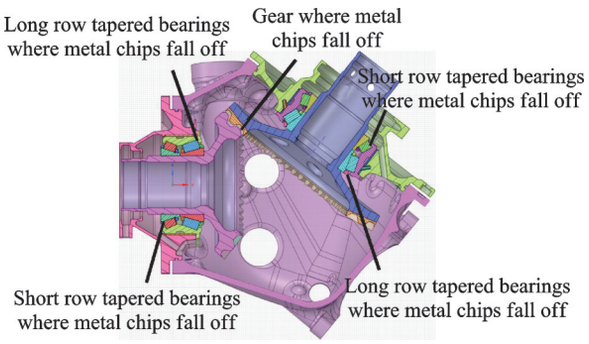

Fig.3 Position distribution of incident particles

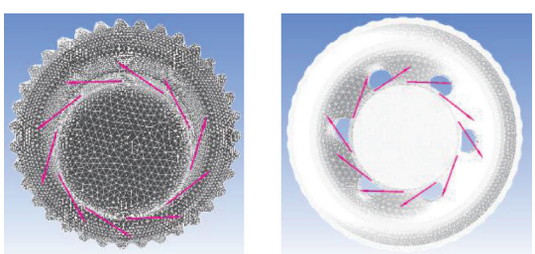

(a) Driving gear (b) Driven gear

Fig.4 Particle velocity vector distribution diagram

The boundary condition of the vent is the pressure outlet, and the particle boundary condition is set as the escape condition. The particle boundary condition of the metal particles signal is set as the absorption condition. All other particle boundary conditions are set as rebound conditions. Using the dynamic grid method to describe the rotational motion of gears, using RNG k-ε turbulence model to adapt to the strong rotating complex flow field inside the intermediate gearbox. The time step is 5×10^{-6} s, and the initial state of the flow field is shown in Fig.5. The initial immersion depth is 17 mm (calculated from the bottom of the driving gear).

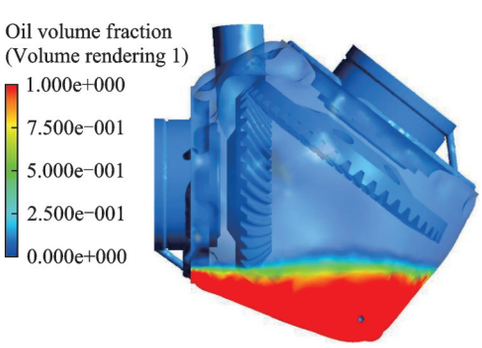

Fig.5 Initial state of the flow field

2 Analysis of Influence of Operating Conditions on Accessibility of Metal Particles

2.1 Analysis of the influence of gear speed

When the gear speed changes, the bearing speed also changes, and the initial motion state of the metal particles also changes. The gear speed is an important factor affecting the motion state of the flow field inside the gearbox, and the motion state of the flow field will directly affect the motion state of the metal particles. Whether adjusting the gear speed can improve the accessibility of metal particles is a problem that must be considered in the study of metal particle accessibility. This section analyzes the impact of input speeds of 3 000, 4 000, 5 000, 6 000, and 7 000 r/min on the accessibility of metal particles.

The particle incident device adopts a single incident particle method, determining each starting point through coordinate points, and shooting one particle in the first time step. The boundary conditions at the vent are set as escape conditions, the particle boundary conditions of the metal particles signal are set as trap conditions, and the other particle boundary conditions are set as reflect conditions.

After calculation, the accessibility of metal particles at different speeds is shown in Table 3.

Table 3 Accessibility of metal particles at different rotational speeds

Speed /(r•min^{-1})	Signal absorption	Vent escape
3 000	0	0
4 000	1	0
5 000	2	1
6 000	4	1
7 000	1	0

At a speed of 3 000 r/min, there is no phenomenon of metal particles being absorbed by the signal or escaping from the vent hole.

At a speed of 4 000 r/min, when the gear rotates for two turns, pinion_8 is absorbed by the signal.

At a speed of 5 000 r/min, when the gear rotates for 17 turns, pinion_9 escapes from the vent, gear_7 is absorbed by the signal, and gear_5 is absorbed by the signal at 18 turns.

At a speed of 6 000 r/min, when the gear rotates for two revolutions, pinion_6 escapes from the vent, pinion_2 and pinion_5 are absorbed by the signal at 10 turns, gear_3 is absorbed by the signal at 17 turns, and gear_7 is absorbed by the signal at 18 turns.

When the gear rotates for three turns at a speed of 7 000 r/min, gear_6 is absorbed by the signal.

Taking the metal particles pinion_1 and gear_1 of the driving gear and the driven gear as examples, Fig.6 shows coordinates and speeds of pinion_1 in the X, Y, and Z directions at different input speeds. Fig.7 shows coordinates and speeds of gear_1 in the X, Y, and Z directions at different input speeds. From Figs.6 and 7, it can be seen that the velocity of pinion_1 in the X direction is negative, but the displacement is in the positive direction of X, at the beginning of the operation of the gearbox. Based on the observation of the intermediate gearbox model, this is because the initial position of the metal particles is near the wall of the bearing cage. After the gear rotates, they start to move and collide with the wall of the cage before rebounding towards the inside of the gearbox.

Combining the motion states of the metal particles in three directions, it is found that the changes do not become more severe with the increase in gear speed. This is because the distribution of lubricating oil in the gearbox also changes after the increase in gear speed. The high viscosity characteristics of lubricating oil hinder the movement of the metal particles. Therefore, except for the sudden change in the speed of the metal particles at the moment of gear rotation, the movement speed of the metal particles at other times is less than 10 m/s. At the same time, it is found that when the driving gear speed is between 4 000—6 000 r/min, the movement state of the metal particles changes the most violently. According to Ref.[33], the lubrication effect inside the gearbox was also good under this working condition, indicating that the distribution of lubricating oil was reasonable at this time, and it would not accumulate at the bottom of the gearbox and immerse the signal. At this time, the probability of the metal particles reaches the area near the signal increased. From Table 3, it can also be seen that the driving gear has the best accessibility of metal particles at 6 000 r/min.

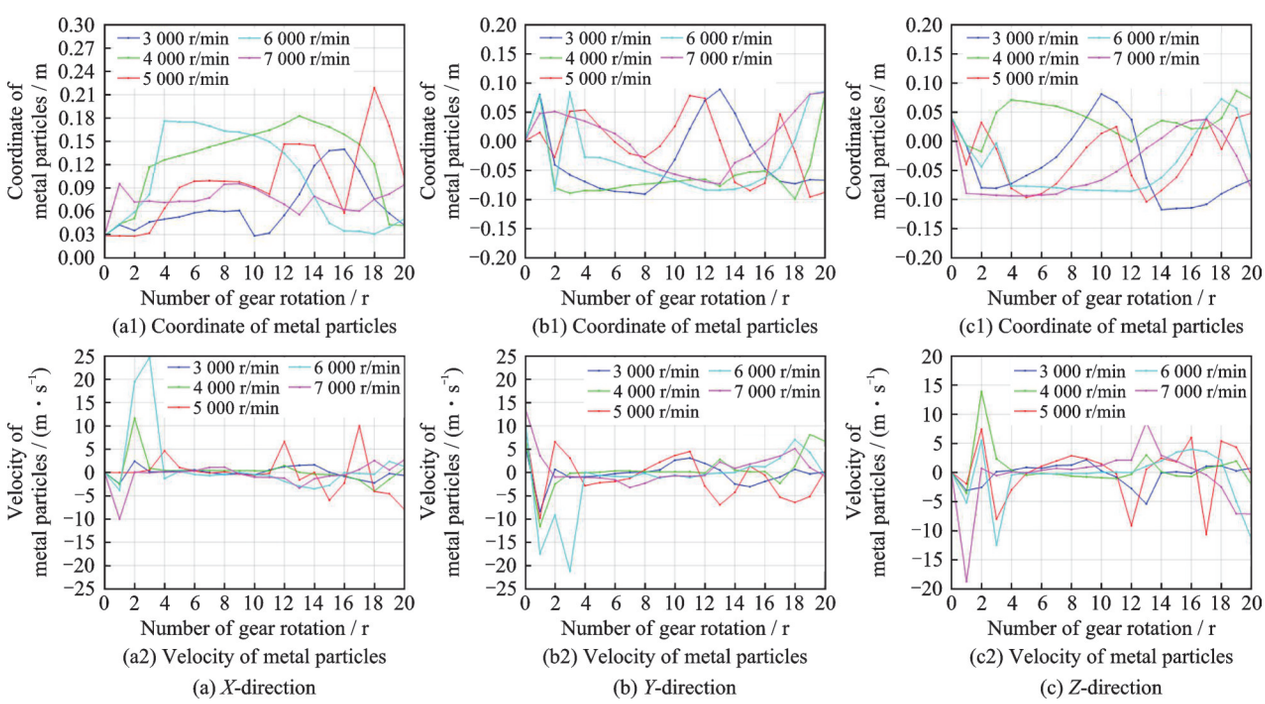

Fig.6 Coordinates and velocities of different gear speeds of pinion_1

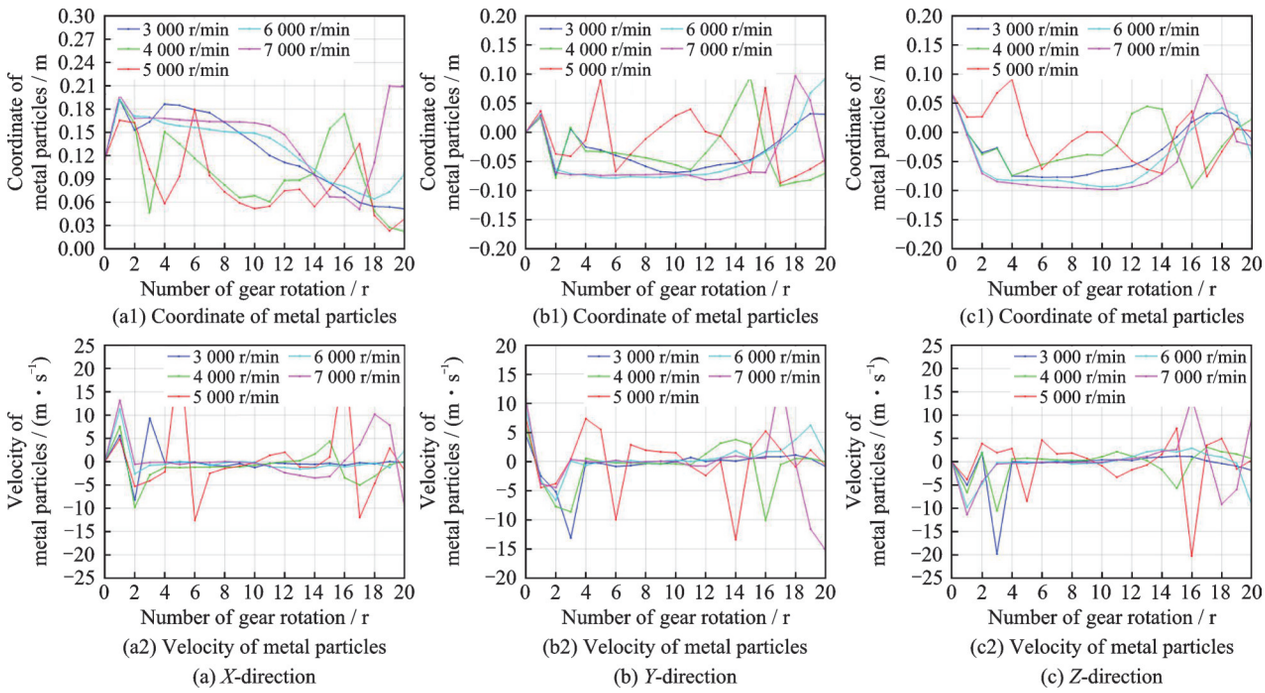

Fig.7 Coordinates and velocities of different gear speeds of gear_1

2.2 Analysis of the influence of lube depth

Due to the high viscosity characteristics of lubricating oil, it is bound to hinder the movement of metal particles in the gearbox. When the amount of lubricating oil is too low, it cannot provide sufficient lubrication and cooling for gears and bearings, resulting in more metal particles generated due to wear. When the amount of lubricating oil is too high, it will increase power loss and cause excessive obstruction to the movement of metal particles, resulting in weakened accessibility. This section analyzes the impact of immersion depths of 10, 17, 24, 31, and 38 mm based on aviation background[34] on the accessibility of metal particles.

After calculation, the accessibility of metal particles at different immersion depths is shown in Table 4.

Table 4 Accessibility of metal particles at different oil immersion depths

Immersion depth/mm	Signal absorption	Vent escape
10	0	2
17	2	1
24	3	1
31	0	1
38	0	1

When the oil immersion depth is 10 mm and the gear rotates for nine turns, gear_7 escapes from the vent hole, when rotating for 17 turns gear_10 escapes from the vent hole.

When the oil immersion depth is 17 mm and the gear rotates for 17 turns, pinion_9 escapes from the vent, gear_7 is absorbed by the signal, gear_5 is absorbed by the signal at 18 turns.

When the oil immersion depth is 24 mm and the gear rotates for 10 turns, gear_10 is absorbed by the signal, pinion_4 is absorbed by the signal at 11 turns, gear_6 is absorbed by the signal at 12 turns, and pinion_2 escape from the vent hole at 16 turns.

When the oil immersion depth is 31 mm and the gear rotates for 18 turns, gear_9 escapes from the vent hole.

When the oil immersion depth is 38 mm and the gear rotates for 10 turns, gear_1 escapes from the vent hole.

Taking the metal particles pinion_1 and gear_1 of the driving gear and the driven gear as examples, Fig.8 shows coordinates and velocities of pinion_1 in the X, Y, and Z directions at different immersion depths. Fig.9 shows coordinates and velocities of gear_1 in the X, Y, and Z directions at different immersion depths. It can be seen that when the immer-

sion depth is small, there is less lubricating oil in the gearbox, and the probability of metal particle movement being hindered by the lubricating oil is small. At this time, the position and velocity gradient of metal particles are relatively violent, and the probability of reaching the area near the signal is also high. But as the immersion depth increases, that is, the volume of the lubricating oil increases, the components are fully lubricated, and the distribution area of the lubricating oil also begins to increase. At this time, the probability of metal particle movement being hindered by the lubricating oil increases, and the position and velocity gradient of the metal particles gradually flattens. Eventually, it may be wrapped and attached to the casing wall by the lubricating oil, resulting in poor accessibility. Among them, when the driving gear rotates for nine turns, gear_1 has already escaped from the gearbox at the

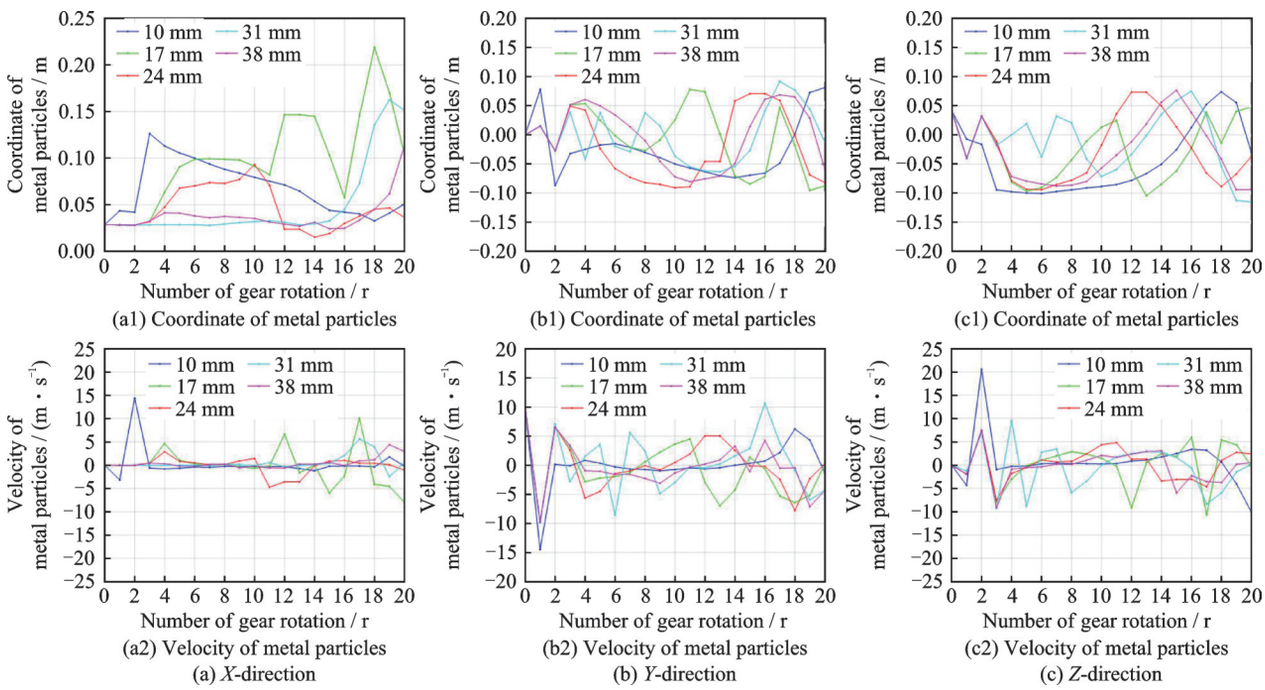

Fig.8 Coordinates and velocities of different oil immersion depths of pinion_1

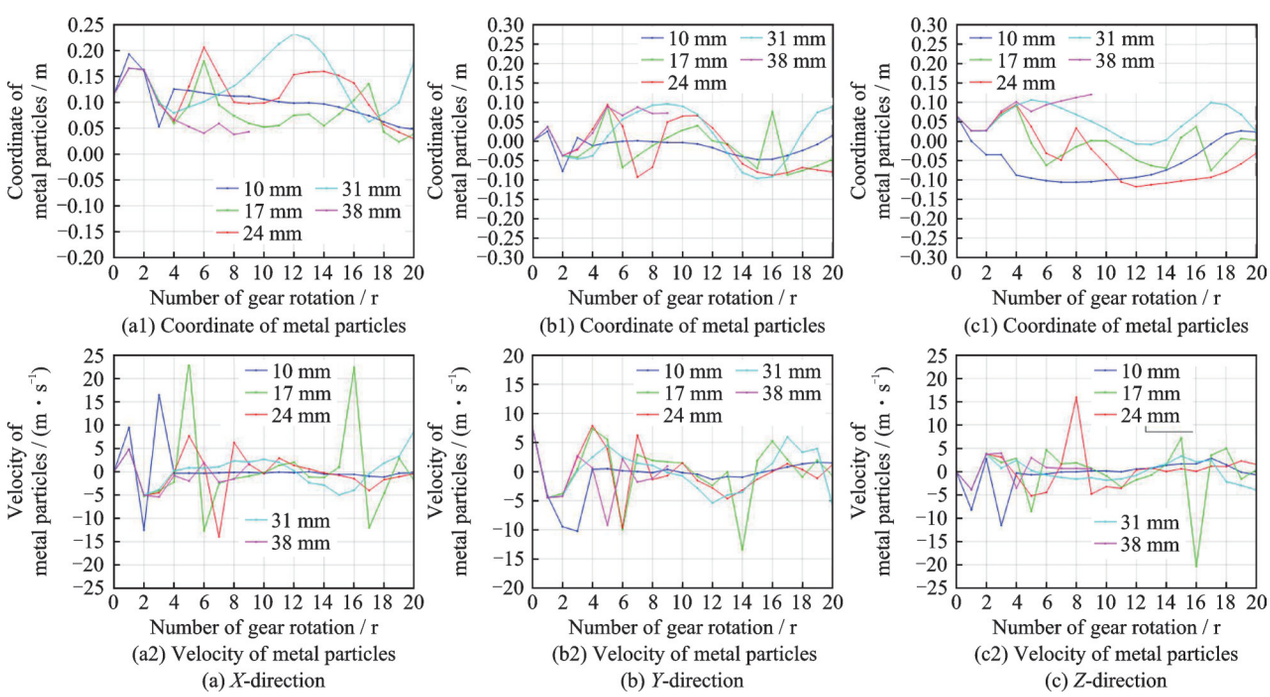

Fig.9 Coordinates and velocities of different oil immersion depths of gear_1

vent hole. According to Table 4, when the immersion depth is 24 mm, the accessibility of metal particles is better, and the lubrication situation inside the gearbox is also better.

3 Influence of Metal Particle Parameters on Accessibility of Metal Particles

3.1 Analysis of the impact of particle size

In addition to the working conditions of the gearbox itself, this article also focuses on exploring the influence of metal particle parameters on its motion state and accessibility. Therefore, this section analyzes the impact of metal particles particle sizes of 0.3, 0.5, 0.72, 1, and 1.2 mm based on aviation background on the accessibility of metal particles.

After calculation, the accessibility of metal particles with different particle sizes is shown in Table 5.

When the particle size is 0.3 mm and the gear rotates for five turns, pinion_7 escapes from the vent hole.

When the particle size is 0.5 mm, there is no phenomenon of metal particles being absorbed by the signal or escaping from the vent hole.

Table 5 Accessibility of metal particles under different particle sizes

Particle size/mm	Signal absorption	Vent escape
0.3	0	1
0.5	0	0
0.72	2	1
1.0	2	0
1.2	0	0

When the particle size is 0.72 mm and the gear rotates for 17 turns, pinion_9 escapes from the vent hole, gear_7 is absorbed by the signal, and gear_5 is absorbed by the signal at 18 turns.

When the particle size is 1.0 mm and the gear rotates for 14 turns, pinion_2 is absorbed by the signal, and pinion_4 is absorbed by the signal at 20 turns.

When the particle size is 1.2 mm, there is no phenomenon of metal particles being absorbed by the signal or escaping from the vent hole.

Taking the metal particles pinion_1, gear_1 of the driving gear and the driven gear as examples respectively, Fig.10 shows the coordinates and velocities of pinion_1 in the X, Y, and Z directions under different metal particle sizes. Fig.11 shows coordinates and velocities of gear_1 in the X, Y, and Z directions under different metal particle sizes. It can

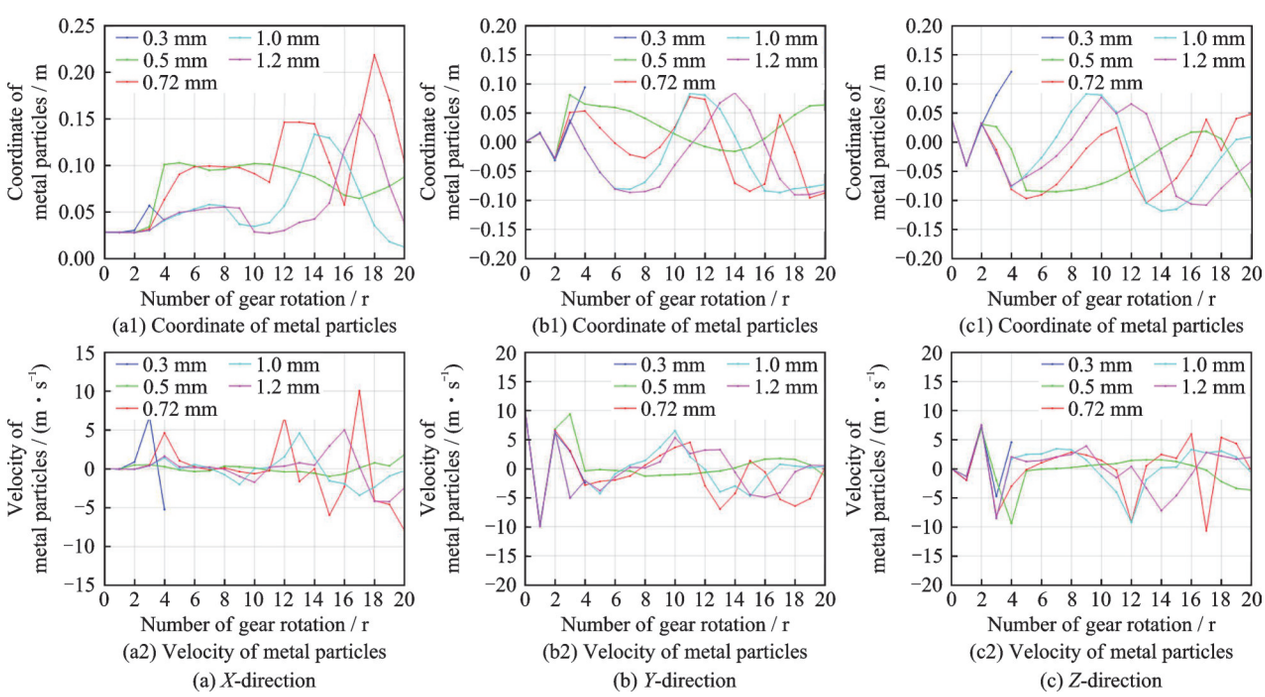

Fig.10 Coordinates and velocities of different metal particle sizes of pinion_1

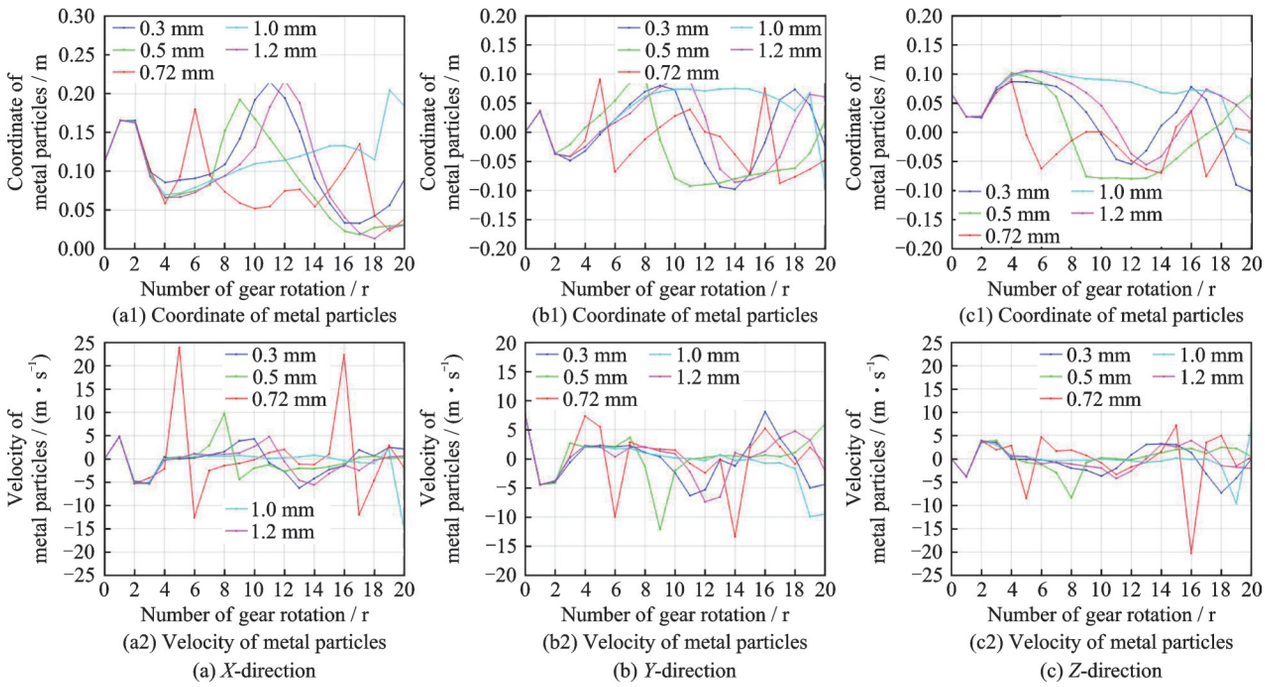

Fig.11 Coordinates and velocities of different metal particle sizes of gear_1

be seen that there is no obvious linear relationship between the accessibility of metal particles under the premise of countless changes in their particle size. This is because although changes in particle size can have a certain impact on the volume and mass of metal particles. if there are countless changes in mass, the drag force and related additional force caused by the flow field on the metal particles are still the main factors affecting their motion state.

3.2 Analysis of the impact of density

If the density of metal particles changes, their mass will also change accordingly, and the degree of influence of the flow field inside the gearbox on their motion state may also be affected, resulting in their accessibility. Therefore, this section analyzes the impact of metal particle density at 7 000, 7 400, 7 810, 8 200, and 8 600 kg/m^3 based on aviation background on the accessibility of metal particles.

After calculation, the accessibility of metal particles with different densities is shown in Table 6.

Table 6 Accessibility of metal particles under different densities

Density/(kg•m^{-3})	Signal absorption	Vent escape
7 000	0	4
7 400	2	1
7 810	2	1
8 200	0	0
8 600	0	0

When the density of the particle is 7 000 kg/m^3 and the gear rotates for nine turns, pinion_2 escapes from the vent hole. When the gear rotates for 11 turns, pinion_3 escapes from the vent hole. When the gear rotates for 13 turns, pinion_4 escapes from the vent hole. When the gear rotates for 15 turns, pinion_6 escape from the vent hole.

When the density of the particle is 7 400 kg/m^3 and the gear rotates for 10 turns, pinion_4 is absorbed by the signal. When the gear rotates for 19 turns, gear_7 escapes from the vent hole. When the gear rotates for 20 turns, pinion_9 is absorbed by the signal.

When the density of the particle is 7 810 kg/m^3 and the gear rotates for 17 turns, pinion_ 9 escapes from the vent, gear_7 is absorbed by the signal, and gear_5 is absorbed by the signal at 18 turns.

When the density of particles is 8 200 kg/m^3 or 8 600 kg/m^3, there is no phenomenon of metal particles being absorbed by the signal or escaping from the vent hole.

Taking the metal particles pinion_1, gear_1 of the driving gear and the driven gear as examples respectively, Fig.12 shows the coordinates and veloci-

ties of pinion_1 in the X, Y, and Z directions at different metal particle densities. Fig.13 shows coordinates and velocities of gear_1 in the X, Y, and Z directions at different metal particle densities.

From Figs.12, 13, and Table 6, it can be seen that the density of metal filings is small and the mass is light. Metal filings are easily affected by high-speed rotating gears and escape from the gearbox through the ventilation hole. The driven gear bearing is not in a horizontal direction but incline towards the bottom of the gearbox, so it is not easy to be blown out. As the density of the particles increases, their gravity undergoes a significant change, which has an increasingly significant impact on their motion state. They are not easily affected by the rotating flow field and escape the gearbox. The degree of change in motion state is also gradually increasing, and the accessibility is also weakened.

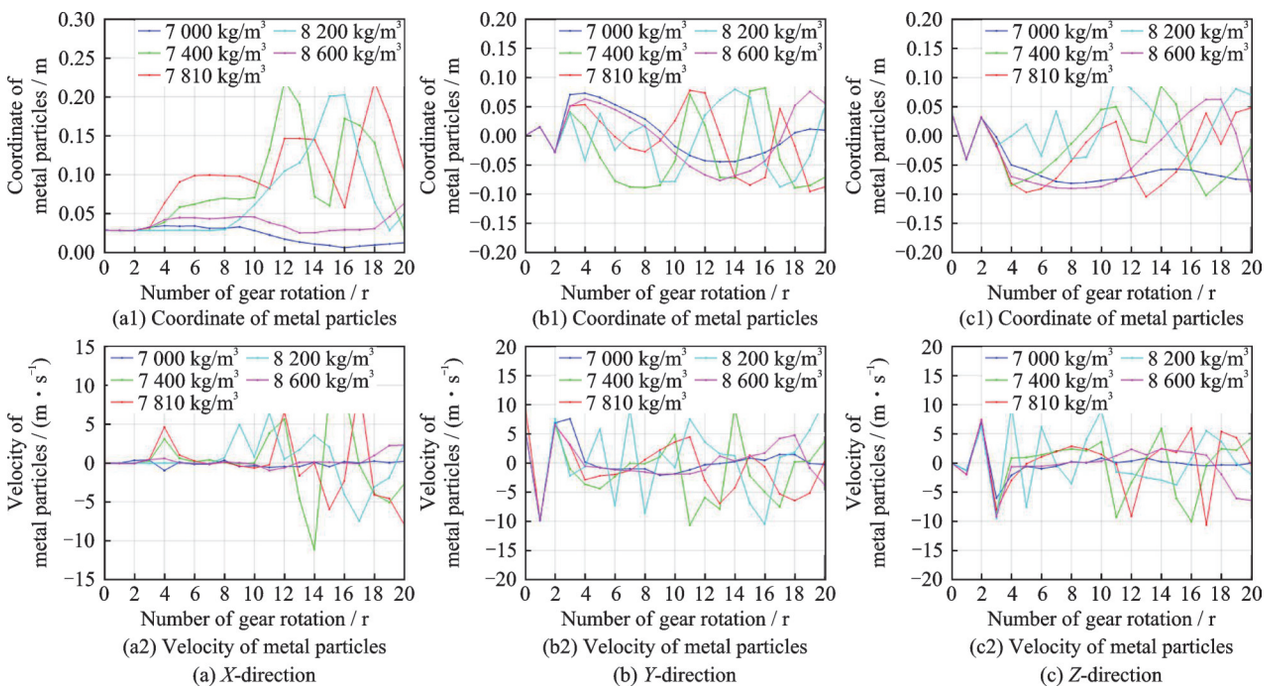

Fig.12 Coordinates and velocities of different densities of pinion_1

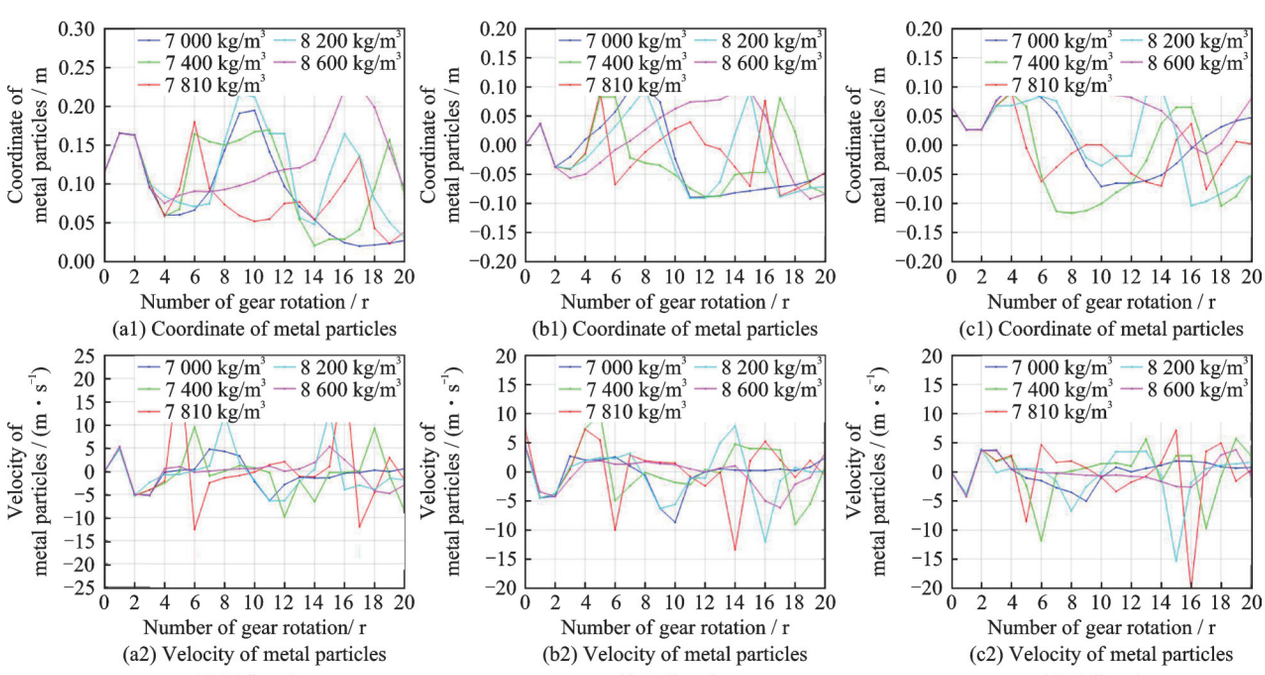

Fig.13 Coordinates and velocities of different densities of gear_1

4 Optimization of Intermediate Gearbox Structure

According to the simulation results of metal particles, it can be concluded that under the current intermediate gearbox structure, metal particles are easily blocked by the casing wall in the case of solid-liquid gas three-phase flow, and the accessibility of metal particles is weak. Based on the analysis of the influencing factors on the movement status of metal particles mentioned above, this section proposes improvement suggestions for the intermediate gearbox structure from the perspective of improving the accessibility of metal particles.

4.1 Structural improvement plan

Observing the movement trajectory of metal particles in CFD simulation, it was found that many metal particles were closer to the signal when they moved to the bottom of the gearbox, but could not be captured due to the size of the signal. Alternatively, the particles that should have reached the bottom of the gearbox may collide with the wall of the gearbox, causing a sudden change in the motion trajectory, thereby affecting accessibility.

In response to the above situation, this section proposes two improvement plans for the gearbox structure.

(1) Plan 1

Move the signal from the bottom of the gearbox to the middle of the gearbox wall, considering weight issues and the proximity of the middle of the gearbox wall to the driven gear, to prevent the improved signal from colliding with the driven gear due to vibration. The overall size of the signal has changed from a cylinder with the height of 37 mm and the diameter of 18 mm to a cylinder with the height of 52 mm and the diameter of 36 mm. This solution can capture the metal particles in advance when they hit the wall, as shown in Fig.14. However, this plan needs to balance and reduce the need for quantitative design.

(2) Plan 2

Keeping the position of the signal unchanged and increasing the height of the signal to 100 mm will not affect other components inside the gearbox, and can also increase the probability of particles being captured by the signal. At the same time, it will also increase the overall structural weight. The structural improvement plan is shown in Fig.15.

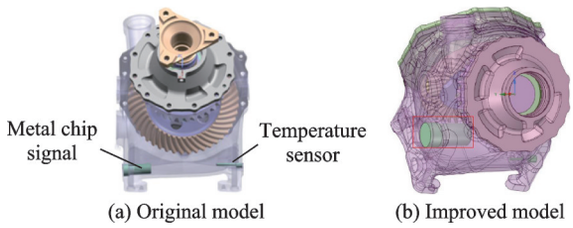

Fig.14 Structural improvement of Plan 1

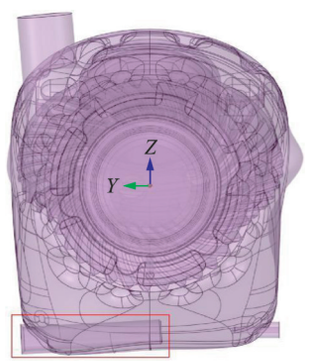

Fig.15 Structural improvement of Plan 2

4.2 Analysis of accessibility of metal particles

The selected working conditions are as follows: The speed is 5 000 r/min, the oil immersion depth is 17 mm, and 10 metal particles are evenly placed at the long row conical bearings. The accessibility of metal particles is studied for the two plans.

(1) Improvement of Plan 1

After calculation, the accessibility of metal particles in Plan 1 is shown in Table 7. By comparison, it was found that before improvement, the metal particles gear_5 and gear_7 were captured by signal, and pinion_9 escaped from the vent hole, and after improvement metal particles pinion_8 and gear_1 escaped from the vent.

The improved motion trajectory of metal particles is shown in Fig.16. Except for two metal parti-

Table 7 Accessibility of metal particles for Plan 1

Accessibility	Signal absorption	Vent escape
Before improvement	2	1
After improvement	0	2

cles escaping from the air hole (as indicated in the yellow box on the left in Figs.16(a,b)), the metal particles flying out of the long row conical bearing of the driving gear collide with the wall surface of the gearbox on the side where the signal is located, and the area is concentrated near the driving gear (as indicated in the yellow box on the right in Fig.16(a)). The same situation applies to the metal particles flying out of the long row conical bearings of the driving gear (as indicated in the yellow box on the right side of Fig.16(b)), where almost no metal particles collides with the casing wall near the signal device, resulting in the signal device being unable to capture the metal particles, and the accessibility is not as good as the previous casing structure. Therefore, improvement of Plan 1 is not feasible.

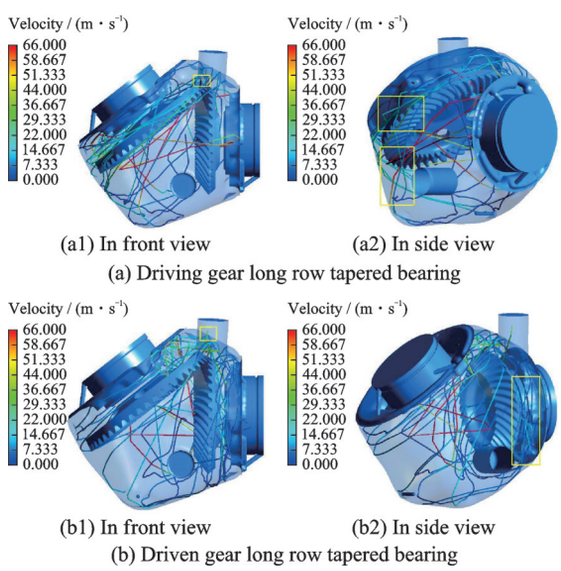

Fig.16 Metal particles motion trajectory of Plan 1

(2) Improvement of Plan 2

After calculation, the accessibility of metal particles in Plan 2 is shown in Table 8. By comparison, it is found that before improvement, gear_5 and gear_7 are captured by signal, pinion_9 escapes from the vent hole. After improvement, pinion_8, pinion_9, pinion_10, gear_1 and gear_6 are captured by signal, pinion_3 escapes from the vent hole.

Table 8 Accessibility of metal particles for Plan 2

Accessibility	Signal absorption	Vent escape
Before improvement	2	1
After improvement	5	1

The improved motion trajectory of metal particles is shown in Fig.17, where the yellow box indicates the trajectory of the metal particles escaping from the gearbox and being absorbed by the signal. When the metal particles move to the bottom of the gearbox, the probability of the metal particles reaching the area near the signal increases greatly due to the elongation of the signal, and the probability of being captured by the signal also increases accordingly. Comparison of the accessibility of three different structures is shown in Table 9. The accessibility of the metal particles in Plan 2 is much better than the structure before the improvement and the Plan 1, therefore, Plan 2 is feasible.

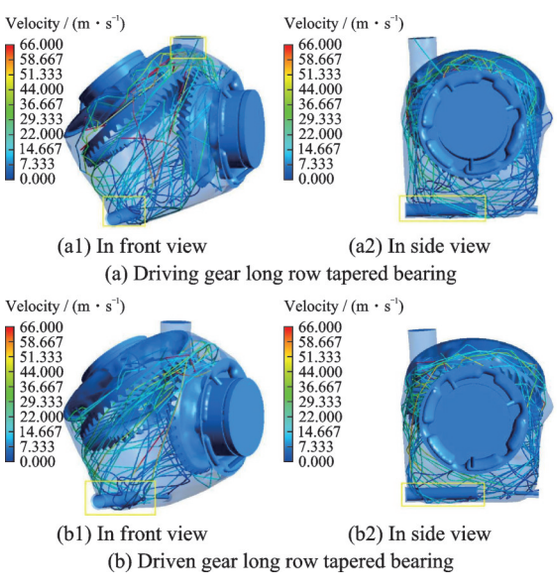

Fig.17 Metal particles motion trajectory of Plan 2

Table 9 Comparison of accessibility of metal particles with three different structures

Accessibility	Signal absorption	Vent escape
Before improvement	2	1
Plan 1	0	2
Plan 2	5	1

5 Conclusions

This paper explores the influencing factors of the movement state and the accessibility of metal particles from two aspects: The intermediate gearbox working condition and the physical parameters of metal particles. A structural improvement plan is proposed for the intermediate gearbox to improve

the accessibility of metal particles. The conclusions are as follows:

(1) When the gear speed is 6 000 r/min or the immersion depth is 24 mm, the accessibility of metal particles reaches the optimal level, and the existing research results have also proven that the lubrication of the gearbox is also optimal at this time.

(2) The particle size of metal particles has a relatively small impact on accessibility without an order of magnitude change. The density and accessibility exhibit a non-linear relationship, and when it is small, it is easy to fly away from the gearbox through the ventilation hole. When the density of metal particles is greater than the original density, accessibility will deteriorate again.

(3) Two schemes are proposed for improving the structure of the intermediate gearbox. Plan 1 shows that after changing the position of the signal, the signal cannot capture the metal chips, and its accessibility is not as good as before, this improvement failed. Plan 2 shows that the probability of metal chips reaching the vicinity of the signal can be increased by lengthening the size of the signal, thereby improving the accessibility of metal chips, without significantly affecting the lubrication condition and weight inside the gearbox.

Due to limited computing resources, this paper studies the accessibility of metal shavings based on the premise of rotating spiral bevel gears 20 times. In future research, it can be combined with exploring the impact of metal shavings on components such as the gearbox, gears, and bearings during their movement in the gearbox, resulting in engraving or damage. Considering the lubrication status and component damage, a more suitable time node for the accessibility of metal shavings can be obtained to enhance the real-time fault monitoring ability and reliability of helicopters. By applying the improvement of Plan 2 proposed in Section 4 of this paper (lengthening the length of the metal terminal signal), the accessibility of the metal terminal can be significantly improved without increasing the overall cost of the receiver, thereby enhancing the reliability of the helicopter.

References

[1] JIANG Yiyao, HU Xiaozhou, SUN Kai, et al. Analysis of flow field characteristics of medium reducer with splash lubrication in a certain helicopter[J]. Journal of Aerospace Power, 2018, 33(12): 3032-3040. (in Chinese)

[2] LUO Pan, ZHANG Bo, WU Wenmin, et al. Simulation study on gear splash lubrication and temperature field[J]. Automobile Technology, 2019(9): 42-48. (in Chinese)

[3] PENG Qianlei, GUI Liangjin, FAN Zijie. Gear splash lubrication numerical simulation and validation based on teeth-face-moving method[J]. Transctions of the Chinese Society of Agricultural Engineering, 2015, 31(10): 51-56. (in Chinese)

[4] LIU Zhongling, FAN Naize, TIAN Huajun, et al. Numerical simulation of the flow field characteristic of lubricating oil in the gearbox of high speed locomotive[J]. Journal of Mechanical Transmission, 2017, 41(3): 129-133. (in Chinese)

[5] DONG Chunfeng, LIN Tengjiao, HE Zeyin. Numerical simulation of flow field in the gearbox based on moving mesh[J]. Mechanical Research & Application, 2011, 24(2): 17-19. (in Chinese)

[6] ZHANG Zhibin. Temperature field and pressure field digital simulation of transmission gear for locomotives[D]. Chengdu: Southwest Jiaotong University, 2011. (in Chinese)

[7] WANG Zhongda. Simulation analysis on fluid and temperature field of bevel gears based on heat-fluid coupling[D]. Changchun: Jilin University, 2015. (in Chinese)

[8] LIU Hua, ARFAOUI G, STANIC M, et al. Numerical modelling of oil distribution and churning gear power losses of gearboxes by smoothed particle hydrodynamics[J]. Proc IMechE Part J: J Engineering Tribology, 2019, 233(1): 74-86.

[9] LI L, VERSTEEG H K, HARGRAVE G K, et al. Numerical investigation on fluid flow of gear lubrication[J]. SAE International Journal of Fuels and Lubricants, 2009, 1(1): 1056-1062.

[10] PENG Qianlei, GUI Liangjin, FAN Zijie. Numerical and experimental investigation of splashing oil flow in a hypoid gearbox[J]. Engineering Applications of Computational Fluid Mechanics, 2018, 12(1): 324-333.

[11] XU Qian, ZHANG Senbo, YANG Konghua, et al. Strategy of directional oil transport for splash lubrica-

tion systems[J]. International Journal of Mechanical Sciences, 2024, 269: 109059.

[12] HU Bingtao, ZHU Rongtao, LI Chaoyong, et al. Simulation study on erosion failure of elbow and analysis of influencing factors[J]. Journal of Changzhou University, 2019, 31(2): 27-34. (in Chinese)

[13] HE Qigong, LIU Xinqiang. The numerical simulation of solid particles invading and distribution in the hydraulic spool valve cap[J]. Chinese Hydraulics & Pneumatics, 2014(10): 99-102. (in Chinese)

[14] QIN Shuaishuai, WANG Licheng, SHEN Shizhong, et al. Measurement and simulation of mixing time of three-phase flow field in the stirred tank[J]. Chemical Reaction Engineering and Technology, 2017, 33(1): 65-72. (in Chinese)

[15] ZHAO Zhiguo, SHI Boqiang, LI Yan, et al. Analysis of movement flow of centrifuge granule based on fluent[J]. Coal Mine Machinery, 2011, 32(3): 112-114. (in Chinese)

[16] SUN Maochuan. The study of micro-partical movement characteristics in multiphase flow system[D]. Chengdu: Southwest Jiaotong University, 2017. (in Chinese)

[17] PENG Li, SHI Zhansheng, DONG Fang, et al. Influence on performance parameters of cyclone sparators based on CFD-DPM[J]. Integrated Intelligent Energy, 2020, 42(12): 43-48. (in Chinese)

[18] ZHANG Tao, ZENG Xianjin, GUO Jianchun, et al. Numerical simulation on oil-water-particle flows in complex fractures of fractured-vuggy carbonate reservoirs[J]. Journal of Petroleum Science and Engineering,2022, 208: 109413.

[19] GAO Xiaojun, ZHOU Zongyan, XU Yang, et al. Numerical simulation of particle motion characteristics in quantitative seed feeding system[J]. Powder Technology, 2020, 367: 643-658.

[20] WANG Huakun, YU Yang, YU Jianxing, et al. Numerical simulation of the erosion of pipe bends considering fluid-induced stress and surface scar evolution[J]. Wear, 2019(440/441): 203043.

[21] ZHANG Yong, CHANG Qi, GE Wei. Coupling DPM with DNS for dynamic interphase force evaluation[J]. Chemical Engineering Science, 2021, 231: 116238.

[22] PAN Hui, CHEN Xizhong, LIANG Xiaofei, et al. CFD simulations of gas-liquid-solid flow in fluidized bed reactors—A review[J]. Powder Technology, 2016, 299: 235-258.

[23] YANG Yan, WEN Chuang. CFD modeling of particle behavior in supersonic flows with strong swirls for gas separation[J]. Separation and Purification Technology, 2017, 174: 22-28.

[24] SUN Xiaoyang, CAO Xuewen. Impact of inter-particle collision on elbow erosion based on DSMC-CFD method[J]. Petroleum Science, 2021, 18(3): 909-922.

[25] SONG Chengming, PEI Binbin, JIANG Mengting, et al. Numerical analysis of forces exerted on particles in cyclone separators[J]. Powder Technology, 2016, 294: 437-448.

[26] ZHU Shuai, ZHAO Qiuyue, LI Xiaolong, et al. CFD simulation of gas-slag-metal multiphase flow in a side-blown vortex smelting reduction reactor[J]. Journal of Sustainable Metallurgy, 2023, 9(3): 1033-1049.

[27] OSMAN K. Numerical investigation on pulse detonation engine performance under different equivalence ratio[J]. Advanced Engineering Letters, 2024, 3(1): 1-12.

[28] YAN Chao. Achievements and predicaments of CFD in aeronautics in past forty years[J]. Acta Aeronautica et Astronautica Sinica, 2022, 43(10): 29-65. (in Chinese)

[29] PRANDTL L, OSWATITSCH K, WIEGHARDT K. Führer durch die Strömungslehre[M]. [S.l.]: Springer-Verlag, 2013.

[30] GOSMAN A D, LOANNIDES E. Aspects of computer simulation of liquid-fueled combustors[J]. Journal of energy, 1983, 7(6): 482-490.

[31] GOSMAN A D, LOANNIDES E. Aspects of computer simulation of liquid-fuelled combustor[J]. AIAA Journal, 1981, 81: 482-490.

[32] MORSI S A, ALEXANDER A J. An investigation of particle trajectories in two-phase flow systems[J]. Journal of Fluid Mechanics, 1972, 55(2): 193-208.

[33] WANG Meng. Research on two-phase flow and heat transfer of the intermediate gearbox in a helicopter under splash lubrication[D]. Nanjing: Nanjing University of Aeronautics and Astronautics, 2021. (in Chinese)

[34] LU Fengxia, WANG Meng, WANG Chunlei, et al. Analysis and optimization method for flow field of intermediate gearbox splash lubrication in helicopters [J]. Acta Aeronautica et Astronautica Sinica, 2020, 41(11): 164-174. (in Chinese)

Acknowledgements This study was supported by the National Natural Science Foundation of China(No.52075241),

and the National Key Laboratory of Science and Technology on Helicopter Transmission (Nanjing University of Aeronautics and Astronautics) (Nos. HTL-A-22K04 and HTL-O-21G13).

Author Prof. **LU Fengxia** received her Ph. D. degree in mechanical engineering from Nanjing University of Aeronautics and Astronautics. She is mainly engaged in research on the application foundation and key technologies of helicopter transmission technology and civil aviation engines, focusing on research directions, such as heat generation and transfer, friction and lubrication, and dynamic analysis.

Author contributions Prof. **LU Fengxia** designed the study and revised the paper. Mr. **WANG Honglin** wrote the manuscript and contributed to the data and figures. Mr. **WEI Kun** contributed to data for the simulation analysis of helicopter gearbox. Dr. **LENG Sheng** contributed to the discussion and background of the study. All authors commented on the manuscript draft and approved the submission.

Competing interests The authors declare no competing interests.

(Production Editor: SUN Jing)

直升机中减速器金属颗粒可及性因素研究及结构优化

陆凤霞，王泓林，韦　坤，冷　晟

（南京航空航天大学直升机传动技术国家级重点实验室，南京 210016，中国）

摘要：直升机中间减速器在飞溅润滑下运转，轴承若因润滑不充分或磨损产生金属屑末，其能否被机匣底部的金属屑末信号器吸附报警直接关系到直升机的飞行安全。为此，本文基于CFD仿真分析方法，应用RNG k-ε湍流模型及动网格技术，采用流体体积法-离散相模型(Volume of fluid-discrete phase model, VOF-DPM)耦合模型，分析金属屑末可达性的影响因素，并对机匣结构开展优化研究。结果表明：齿轮转速在6 000 r/min或浸油深度在24 mm时，金属屑末可达性最佳；金属屑末的密度与其可达性呈非线性关系，粒径在未发生数量级变化的前提下对其可达性影响较小。

关键词：减速器；飞溅润滑；金属屑末；CFD；三相流